



THE UNIVERSITY *of* EDINBURGH

Edinburgh Research Explorer

Large-scale experiments on the behaviour of a generalised Oscillating Water Column under random waves

Citation for published version:

Viviano, A, Naty, S, Foti, E, Bruce, T, Allsop, W & Vicinanza, D 2016, 'Large-scale experiments on the behaviour of a generalised Oscillating Water Column under random waves', *Renewable Energy*, vol. 99, pp. 875-887. <https://doi.org/10.1016/j.renene.2016.07.067>

Digital Object Identifier (DOI):

[10.1016/j.renene.2016.07.067](https://doi.org/10.1016/j.renene.2016.07.067)

Link:

[Link to publication record in Edinburgh Research Explorer](#)

Document Version:

Peer reviewed version

Published In:

Renewable Energy

General rights

Copyright for the publications made accessible via the Edinburgh Research Explorer is retained by the author(s) and / or other copyright owners and it is a condition of accessing these publications that users recognise and abide by the legal requirements associated with these rights.

Take down policy

The University of Edinburgh has made every reasonable effort to ensure that Edinburgh Research Explorer content complies with UK legislation. If you believe that the public display of this file breaches copyright please contact openaccess@ed.ac.uk providing details, and we will remove access to the work immediately and investigate your claim.



Large-scale experiments on the behaviour of a generalised oscillating water column under random waves

Antonino Viviano^a, Stefania Naty^a, Enrico Foti^a, Tom Bruce^b, William Allsop^c, Diego Vicinanza^d

^a*Department of Civil Engineering and Architecture, University of Catania. Via S. Sofia 64, 95123 Catania, Italy*

^b*Institute for Energy Systems, School of Engineering, The University of Edinburgh, Kings Buildings, Mayfield Rd, Edinburgh EH9 3JL, United Kingdom*

^c*Coastal Structures Group, HR Wallingford, Howbery Park, Wallingford, OX10 8BA, United Kingdom*

^d*Dipartimento di Ingegneria Civile, Design, Edilizia e Ambiente, Seconda Università di Napoli, Via Roma 29, 81031 Aversa (Caserta), Italy*

Abstract

This work investigates wave reflection and loading on a generalised Oscillating Water Column (OWC) wave energy converter by means of large scale (approximately 1:5-1:9) experiments in the Grosse Wellenkanal (GWK), in which variation of both still water depth and orifice (PTO) dimension are investigated under random waves. The model set-up, calibration methodology, reflection analyses and loadings acting on the OWC are reported. On the basis of wave reflection analysis, the optimum orifice is defined as that restriction which causes the smallest reflection coefficient and thus the greatest wave energy extraction. Pressures on the front wall, rear wall and chamber ceiling are measured. Maximum pressures on the vertical walls, and resulting integrated forces, are compared with available formulations for impulsive loading prediction, which showed significant underestimation for

heaviest loading conditions.

The present study demonstrates that a OWC structure can serve as a wave absorber for reducing wave reflection. Thus it can be integrated in vertical wall breakwaters, in place of other perforated low reflection alternatives. The possibility to convert air kinetic into electric energy, by means of a turbine, may give an additional benefit. Thus the installation of such kind of energy converters becomes interesting also in low energy seas.

Keywords: wave energy converter, oscillating water column, physical model, wave reflection

1 Nomenclature

2	δ	thickness of front vertical wall
3	η	free surface elevation
4	ω	generic angular frequency
5	a	draft of front vertical wall
6	A_0	orifice's cross-sectional area
7	A_c	chamber's horizontal cross-sectional area
8	B	longitudinal width of caisson
9	B_t	transverse width of caisson
10	C_r	total reflection coefficient of a random wave train
11	$C_{r(f)}$	spectral reflection coefficient, defined for each wave component of the
12		spectrum

13	d	water depth from caisson floor
14	d_0	orifice diameter
15	f_{In}	complex parameter of n th incident wave component
16	$F_{n,m}$	complex parameter of the m th probe and n th wave component
17	f_{Rn}	complex parameter of n th reflected wave component
18	h	water depth from flume floor
19	H_s^*	significant incident relative wave height $= H_{m0,i}/h$
20	h_i	opening height of front vertical wall
21	h_t	height of caisson chamber
22	$H_{m0,i}$	significant (spectral) height of incident waves, at the paddle
23	k	generic wave number
24	L	generic wave length
25	L_p	wave length (in depth h) based upon peak period
26	m	m th probe
27	n	n th harmonic (wave) component
28	s	approach slope
29	s_w	wave steepness
30	t	time variable

31 T_p peak wave period

32 t_{end} total duration of data

33 x abscissa in the direction of incident wave propagation

34 x_m distance between the general probe and the first one

35 **1. Introduction**

36 In recent years, wave energy exploitation has seen increasing interest
 37 among researchers and government [1, 2, 3, 4, 5, 6]. More than 1000 Wave
 38 Energy Converters (WECs) have been developed and are patented worldwide
 39 [7, 8].

40 One of the main issues for developing these technologies is the economic
 41 aspect. Compared to other renewable technologies, WECs costs are, in fact,
 42 currently still too high. Furthermore, their development is also heavily de-
 43 pendent upon their reliability and operability in open waters, given that
 44 they are exposed to extreme conditions of nature. Critical to their overall
 45 expense are the costs of building and/or installing the WEC devices.

46 A solution to significantly decrease costs would be to develop hybrid de-
 47 vices that can be embedded within coastal or offshore infrastructure. This
 48 important new concept for coastal defence structures could make a realistic
 49 contribution for the WEC systems to become economically competitive with
 50 other renewable energy devices, especially where they can be integrated in
 51 existing or expanding structure. Moreover multi-purpose solutions combin-
 52 ing renewable energy from the sea (wind, wave, tide), aquaculture and trans-

53 portation facilities can be considered as a challenging, yet advantageous, way
54 to boost blue growth [9].

55 Two different types of hybrid breakwaters have been developed over the
56 past decades: caisson Oscillating Water Columns (OWC) [10, 11, 12, 13,
57 14, 15, 16, 17, 18, 19] and rubble mound/sea wall Overtopping Devices
58 [20, 21, 22, 23, 24]. In the OWC devices the action of the incident waves
59 induces alternately a compression and an expansion of the air pocket (upper
60 part of the chamber), able to generate an air flow in the air duct connected
61 to the atmosphere. In this duct, a self-rectifying turbine coupled to an elec-
62 trical generator is driven to produce electrical energy. Overtopping devices
63 generally use a slope facing the waves with a reservoir behind to capture the
64 overtopping flows. The energy is extracted via low head hydraulic turbines,
65 using the difference in water levels between the reservoir and the local sea
66 level.

67 Recently, in a breakwater at Mutriku, 16 OWC chambers were formed
68 in a section of vertical wall [16]. These chambers were however damaged
69 in storms in 2007, 2008 and (most seriously) in 2009. Some of the causes
70 of the damage have been described [17, 25]. This failure has particularly
71 demonstrated the need for more research to quantify loadings on and around
72 these devices.

73 In the context of WECs, OWC devices considered here have the advantage
74 of simplicity, since the only moving part of the energy conversion mechanism
75 is the turbine rotor, which is located above the water level [26]. Despite their
76 relative simplicity, OWC caissons involve complex hydrodynamics as they re-
77 spond to wave motion. Such a complexity has been highlighted in [27] by flow

78 visualization experiments, demonstrating that large vortices develop around
79 the front “curtain” wall and internal sloshing occurs during the inflow period.
80 Additionally, internal breakers have been observed indicating that loads on
81 the back wall might be considerably higher than would be anticipated from
82 assumed (pulsating) wave motions.

83 The flow complexity highlights the importance of analyzing both wave
84 motion and loadings at the OWC caisson. Such analyses were first carried
85 out experimentally by Takahashi [10]. He determined that wave reflections
86 from an efficient OWC device can be relatively small and that its stability
87 against storms is high. Additionally he proposed an analysis method for
88 loads on the caisson, considering the influence of air pressure in the cham-
89 ber. The incident and reflected wave heights in front of OWC have been
90 investigated experimentally with monochromatic waves in [28]. The aim of
91 that study was to estimate the rate of conversion of incident wave energy
92 into pneumatic energy (in the air column) and the influence of turbine. The
93 Authors concluded that the energy of the air increases and the reflection co-
94 efficient reduces with a turbine. Such results imply some correlation between
95 the wave reflections and the air outflow characteristics. Other experiments,
96 carried out with random waves [29], give values of reflection coefficient in
97 front OWC devices when operating efficiently between $C_r = 0.40$ and 0.54 .

98 OWC hydrodynamics are mainly affected by chamber geometry and tur-
99 bine pneumatic damping (pressure difference across the turbine). The im-
100 portance of considering the coupling effect between chamber and air turbine
101 has been investigated in [30], identifying that the performances of these two
102 elements depend on each other. In particular, the turbine must provide the

103 optimal pneumatic damping in order to achieve (near-)resonant conditions
104 in the chamber. In turn, the chamber must provide the maximum pneu-
105 matic energy to maximize energy extraction. The effect of the turbine on
106 air flow inside the chamber is frequently modelled [31] by inserting a restric-
107 tion (orifice) whose dimensions can be easily varied, so varying the resulting
108 damping.

109 Evaluation of the loadings induced by waves acting on OWC caisson
110 breakwaters have been reported in [32], using small scale experiments. In
111 particular, the Authors found that wave pressures on OWC caisson break-
112 waters are smaller than the wave pressure at vertical wall when compared
113 with the well-known Sainflou [33] and Goda [34] empirical formulas for ver-
114 tical wall breakwaters. Under the wave conditions tested, it was found that
115 Sainflou's formula [33] overestimated the wave pressures acting on an OWC
116 caisson breakwater; whereas Kuo et al. [32] found that Goda's formula [34]
117 provided good estimation for the horizontal force, but tends to underestimate
118 the overturning moment. Other experiments for estimating wave forces on
119 OWC have been carried out by Ashlin et al. [35], for regular waves. They
120 observed that the peak horizontal wave force acting on the structure can be
121 more than 2.5 to 3 times the peak vertical wave force. Moreover the non-
122 linearity due to the variation in the wave steepness in the case of vertical
123 forces is found slightly more compared to the horizontal forces.

124 In the present contribution, results of unique large scale tests (at ap-
125 proximately 1:5 to 1:9 of full scale) are presented, in order to give useful
126 information on wave reflection and loadings acting on an OWC breakwater
127 under random waves. Such tests were supported by HYDRALAB IV [36]

and were carried out at the Large Wave Channel (GWK) of the Coastal Research Centre (FZK) in Hannover. The details of experimental setup are reported in Section 2. Wave reflection estimation and reflection coefficients as function of OWC geometry and wave conditions are discussed in Section 3. Evaluation of loadings on the structure is presented in Section 4. Finally, Section 5 draws together the conclusions.

2. Experimental setup

The OWC device tested was simply a hollow caisson placed at the top of a short approach slope. All the walls are vertical and the front wall is cut off at the bottom in order to form the chamber opening. A cylindrical duct lead upwards from the roof of the caisson. This duct contains a restriction (i.e. an orifice) which enables the simulation of the damping (power take off, PTO) of an air turbine.

Figure 1 shows a sketch and photographs of the tested OWC device, with the main parameters of interest. The parameters and the values which have been tested are shown in Table 1, which also distinguishes between fixed and variable dimensions.

The fixed dimensions are those related to the caisson construction and foundation: slope and berm height; longitudinal and transverse width of the internal caisson; height of the caisson; the front vertical wall opening height and its thickness. Model setup parameters varied were the still water depth (h) and orifice diameter (d_0). The variation of the water depth causes the modification of two other linked measures: water depth with respect to the caisson floor (d), and draft or ‘curtain wall submergence’ of the front wall

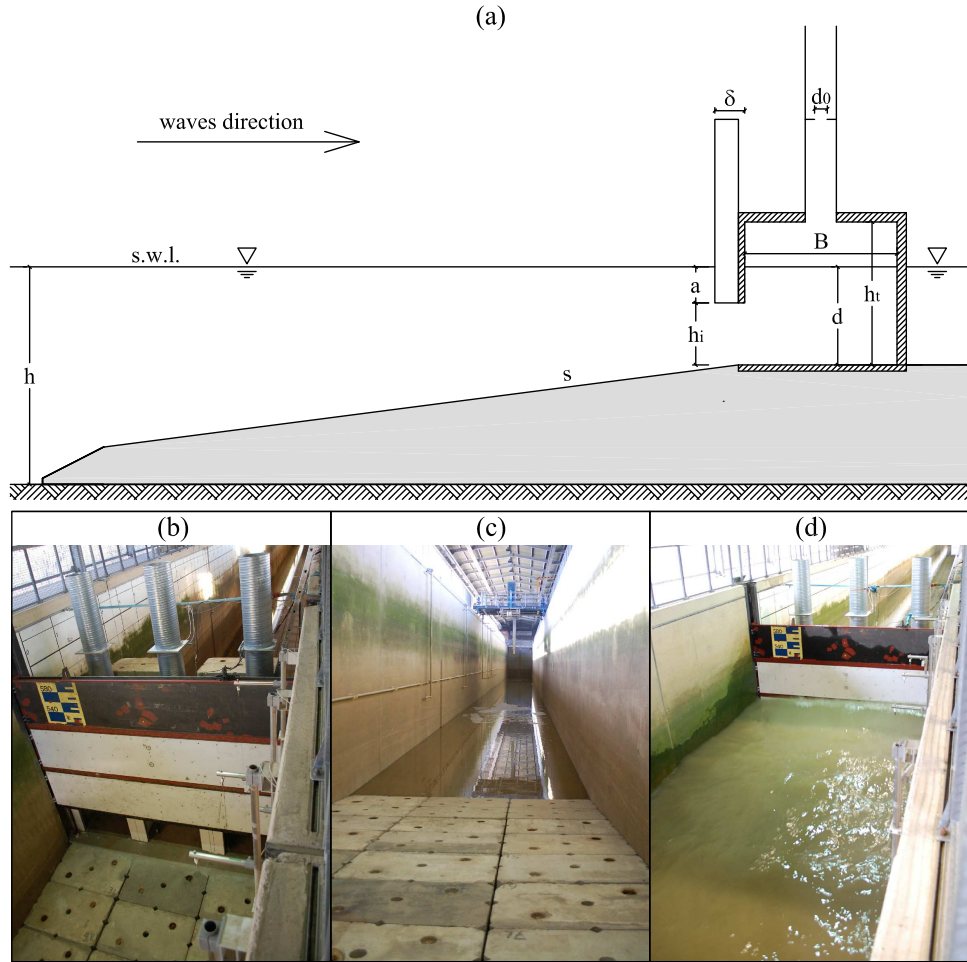


Figure 1: Schematic representation and photos of OWC caisson tested in the GWK: (a) sketch of the tested configuration with main geometrical parameters; (b) view of front wall and opening; (c) photo of foreshore slope towards the wave maker; (d) view of waves in front of the OWC chambers.

Table 1: Description of OWC caisson geometrical parameters for both fixed and variable dimensions.

Geometrical Parameter	Symbol	Tested Value(s)	
Approach slope	s	1:6	Fixed
Height of caisson chamber	h_t	2.30 m	Fixed
Longitudinal width of caisson	B	2.45 m	Fixed
Transverse width of caisson	B_t	1.45 m	Fixed
Thickness of front vertical wall	δ	0.50 m	Fixed
Opening height of the front wall	h_i	1.00 m	Fixed
Orifice diameter	d_0	0 – 0.30 m	Variable
Water depth from flume floor	h	3.00; 3.50 m	Variable
Water depth from caisson floor	d	1.08; 1.58 m	Variable
Draft of front vertical wall.	a	0.08; 0.58 m	Variable

152 (a). As the two water levels tested were different by 0.50 m, d and a have two
 153 values 0.50 m apart. The orifice diameter, d_0 , varies between 0 and 0.3 m,
 154 where the zero value corresponds to full closure of the air duct.

155 Large scale experiments of the described device have been carried out at
 156 the Large wave channel (Grosse Wellenkanal, GWK) of the Coastal Research
 157 Center, in Hannover. The flume is 307 m long, 7 m deep and 5 m wide and
 158 can generate waves having (individual) maximum height of 2 m. The random
 159 waves can reach $H_{m0} \approx 1.3$ m.

160 Air compressibility causes scaling issue in OWC small scale physical mod-
 161 elling, as explored by Weber [37]. For these large scale tests, Webers work
 162 suggests that the influence of scaling (of chamber height and PTO char-
 163 acteristics) upon device performance will be of the order of 10%. A later
 164 paper will compare measurements in small scale tests with these large scale
 165 experiments, and include some detailed comparison with Webers predicted
 166 influences.

167 Three OWC caissons were installed across the full width of the flume,
 168 with the structure's front face 97.47 m from the wave maker. The three
 169 OWC caisson were hydraulically identical although only the central one was
 170 instrumented. A sketch of the flume arrangement at GWK is shown in Fig-
 171 ure 2, with indication of OWC placement and measurement systems outwith
 172 the caisson, in both plan (top) view and longitudinal section. In particular,
 173 eight wave gauges have been placed along the flume; four of them (WG01-
 174 WG04) have been mounted on the flat bottom full depth zone and they have
 175 variable mutual distances in order to be used for evaluating incident and
 176 reflected wave components. The other four wave gauges (WG05-WG08) are

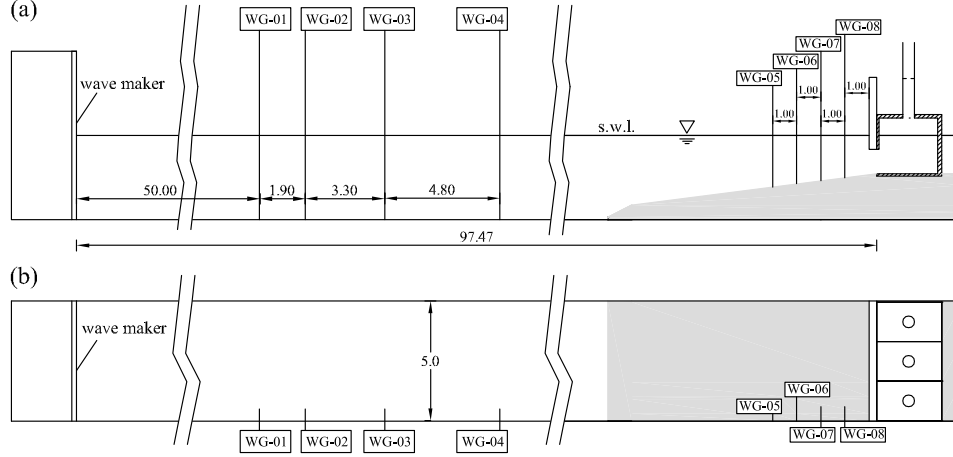


Figure 2: Experimental setup at GWK with indication of wave gauges along the channel: (a) longitudinal section; (b) top view. All dimensions in m.

located near the front wall of the OWC, at intervals of 1 m, with WG08 located 1 m from the wall. Such a packed configuration of near-wall wave probes aims to describe complex wave-structure interactions, also in the presence of breaking waves which may cause impulsive actions. These data have been used in this paper to define the upper limit of the ‘wet’ domain, in order to compute the forces acting on front wall.

The central caisson was equipped with sensors of different types (see Figure 3). Five wave gauges (WG09-WG13) allowed measurement of the chamber water surface motion within the OWC chamber. Pressure sensors were installed in a vertical array on the outer side of front wall (P1-P5), on the rear internal wall facing into the chamber (P8-P12), and in the ceiling, again, looking into the chamber (P6, P7, P13). In such a way it was possible to measure pressure distributions, and infer force-time histories, and to identify

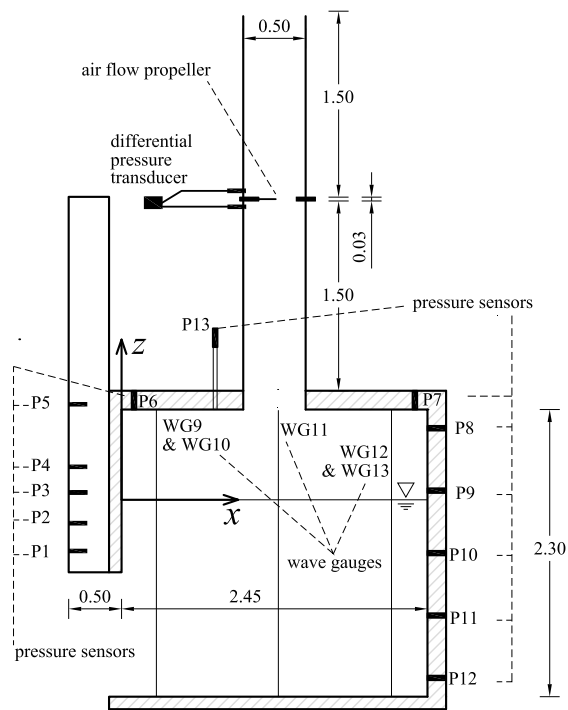


Figure 3: Detailed longitudinal section of the OWC device with location of measurement sensors and of x and z axes. All dimensions in m.

the most loaded points of the structure. A differential pressure transducer and an air flow propeller were located at the orifice of the duct (the ‘chimneys’ in Figures 1b and 1d), in order to analyse the air flow characteristics and to relate them to wave reflection and loadings.

The experiments described here were carried out with both regular and random wave conditions. Only random wave tests are analysed here, since the aim of the present contribution is to study reflection and loadings for an OWC device in realistic sea wave conditions. All the random wave tests, summarised in Table 2, have been carried out using conventional JONSWAP spectra with peak enhancement factor $\gamma = 3.3$. The test matrix of wave height and periods was designed to include tests at the four (nominal) wave steepnesses of $s_w = 0.01, 0.02, 0.03$ and 0.04 . This resulted in peak wave periods between 3.0 and 6.5 s; by significant wave heights from 0.26 to 1.00 m (derived as incident wave heights from the reflection analysis). A total of twelve incident random wave conditions at the paddle were tested with the largest water depth of $h = 3.5$ m, five of which were also tested for $h = 3$ m. The wave steepness values of the tested conditions (shown in Figure 4) are always less than or equal to 0.04.

The full range of the orifice diameter d_0 was explored for only three wave conditions, with different values of T_p and minimum values of h . These tests were performed at the outset, in order to identify an “optimum orifice” which gave the greatest wave energy conversion at the OWC device and, consequently, the least wave reflection. It was established that the “optimum orifice” diameter was 0.2 m, and this value was adopted as a standard for the remaining tests. More details on the wave reflection as function of orifice

Table 2: Tested conditions, obtained by varying: orifice diameter (d_0), peak period (T_p) and nominal significant (spectral) height ($H_{m0,i}$) of incident random waves at the wave maker, still water depth at the wave maker (h), draft of caisson front vertical wall (a).

Test number	d_0 [m]	T_p [s]	$H_{m0,i}$ [m]	h [m]	a [m]
1; 2; 3; 4; 5	0; 0.05; 0.1; 0.2; 0.3	3.0	0.26	3.5	0.58
6	0.2	3.0	0.39	3.5	0.58
7; 8	0; 0.2	3.0	0.52	3.5	0.58
9; 10; 11; 12	0.05; 0.1; 0.2; 0.3	4.0	0.40	3.5	0.58
13; 14	0; 0.2	4.0	0.60	3.5	0.58
15	0.2	4.0	0.80	3.5	0.58
16; 17	0; 0.2	4.5	0.26	3.5	0.58
18; 19; 20; 21; 22	0; 0.05; 0.1; 0.2; 0.3	5.0	0.54	3.5	0.58
23	0.2	5.0	0.81	3.5	0.58
24; 25	0; 0.3	6.0	0.67	3.5	0.58
26	0.2	6.0	1.00	3.5	0.58
27	0.2	6.5	0.40	3.5	0.58
28	0.2	3.0	0.26	3.0	0.08
29	0.2	3.0	0.52	3.0	0.08
30	0.2	4.0	0.60	3.0	0.08
31	0.2	5.0	0.54	3.0	0.08
32	0.2	6.0	0.67	3.0	0.08

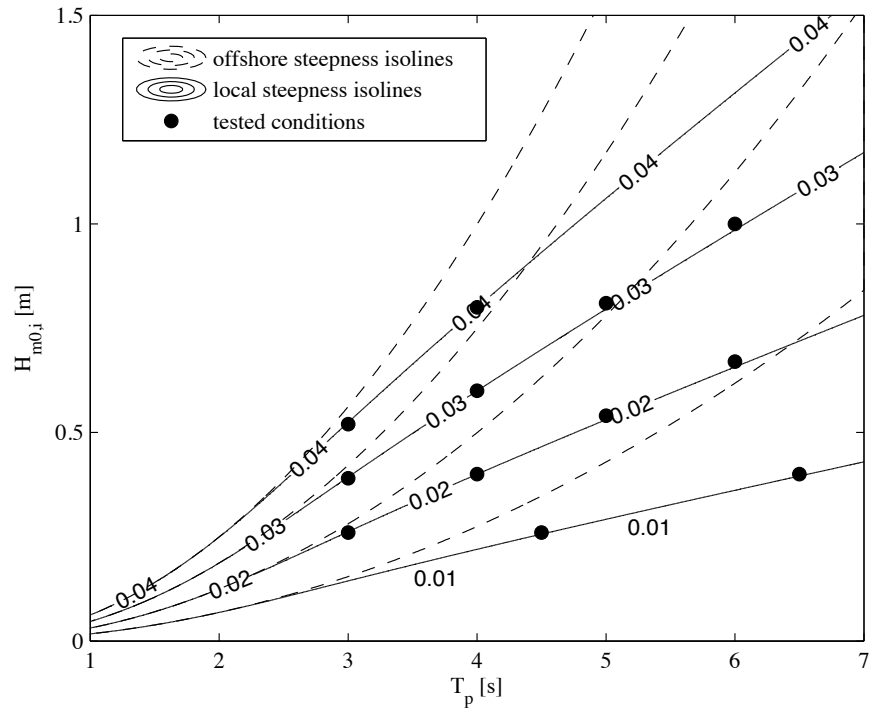


Figure 4: Nominal wave characteristics ($H_{m0,i}$ and T_p) of the tested conditions on lines of constant offshore and local wave steepness; local wave steepness is calculated at depth $h = 3.5$ m, by applying dispersion relation.

diameter are reported in Section 3.2.

3. Wave reflection

A mutual influence is expected to exist between wave motion and OWC:
i) a reduction on wave reflection is expected, with respect to vertical wall breakwaters, since the OWC device is able to convert incident wave energy into (ultimately) kinetic energy of air passing through the orifice; ii) the intensity of wave reflection will have some influence (probably complicated) on the loading of the OWC caisson both on its front face and within the chambers. Wave motion dynamics, addressed in this Section, is preliminary to the loading aspects which are explored in Section 4. In particular, the objective here is the wave reflection estimation as function of: incident wave characteristics, OWC caisson dimensions and air flux restriction due to the orifice.

3.1. Estimation of reflected waves

Wave motion at the wave flume can be separated into incident and reflected components using simultaneous free surface elevations at several wave gauges. The experimental set-up at GWK allowed the use of up to four wave gauges (WG01-WG04) placed in the flat bed zone of the channel, well offshore of the foreshore and OWC. For this reason, an advanced method has been adopted for wave reflection estimation [38] which makes use of data from all the four wave probes. Such a method extends the widely used Mansard and Funke three-probe formulation [39], which is in turn based on the Goda and Suzuki two-probe approach [40]. In detail, the wave field is assumed

238 to be the sum of linear incident and reflected wave components and can be
 239 expressed in complex form as follows:

$$\eta = \sum_{n=-N}^N [f_{In}e^{i(\omega_n t - k_n x)} + f_{Rn}e^{i(\omega_n t + k_n x)}], \text{ for } n \neq 0 \quad (1)$$

240 where: t is the time variable; x is the direction of incident wave propagation;
 241 subscript n is representative of the n th harmonic component; $\omega_n = 2\pi n/t_{end}$
 242 is the discrete angular frequency, where t_{end} is the total duration of data to be
 243 considered; k_n is the wave number obtained from the linear dispersion relation
 244 as function of ω_n and water depth. f_{Rn} and f_{In} are two complex parameters,
 245 defined respectively for reflected and incident waves, whose absolute values
 246 are the amplitudes and their arguments represent the phases.

247 The Fourier transformation, applied at each probe m , allows the wave
 248 signal η_m to be written as a function of a complex parameter $F_{n,m}$, defined
 249 generally for the m th probe and n th harmonic component:

$$\eta_m = \sum_{n=-N}^N F_{n,m}e^{i\omega_n t} \quad (2)$$

250 Moreover, from eq. (1), it is possible to obtain:

$$F_{n,m} = f_{In}e^{-ik_n x_m} + f_{Rn}e^{ik_n x_m} \quad (3)$$

251 where x_m is the position of each probe m ; the origin of the x abscissa can
 252 be placed at the wave probe nearest to wave-maker ($m = 1$), in such a way
 253 that x_m represents the distance between the general probe and the first one
 254 (and consequently $x_1 = 0$).

255 The eq. (3) can be applied to each probe to obtain, for the generic n th
 256 harmonic, a system of m linear equations in which f_{In} and f_{Rn} are the only

257 unknowns. If $m = 2$, i.e. only two probes are used, such a system can be
 258 easily solved since it is composed by two equations and two unknowns. The
 259 determinant of such a system vanishes for $x_2/L_n = 0.5$. Therefore, to obtain
 260 reliable results using this method, the ratio x_2/L_n should be in the range
 261 of $0.05 - 0.45$. This limitation is important, especially for random waves,
 262 because it is not easily satisfied for each component of the spectrum. If
 263 $m > 2$, least square method can be used and the results are more stable, also
 264 for random waves.

265 Absolute values of f_{In} and f_{Rn} are proportional to incident and reflected
 266 wave amplitudes of the n th harmonic, respectively. Thus the spectral re-
 267 flection coefficient $C_{r(f)}$, related to the angular wave frequency component
 268 ω_n , and the total reflection coefficient C_r of a random wave train can be
 269 computed, respectively, as follow:

$$C_{r(f)} = \frac{|f_{Rn}|}{|f_{In}|} \quad (4)$$

270

$$C_r = \sqrt{\frac{\sum_{n=n_1}^{n_2} |f_{Rn}|^2}{\sum_{n=n_1}^{n_2} |f_{In}|^2}} \quad (5)$$

271 where n_1 and n_2 are, respectively, the lower and upper bounds of the spectral
 272 range used to compute the reflection coefficient.

273 The formulation summarized above is described in detail in [38], in which
 274 it was applied for $m = 2; 3; 4$, i.e. for two, three and four wave probes.
 275 The finding was that three- and four- probe methods yield similar values,
 276 but the four-probe method reduces the effect of measurement errors with
 277 respect to the more familiar three- probe method, proposed in [39]. The two
 278 probe method produces a false reflection coefficient when the wave spectrum
 279 frequency range is wide, so is not considered further here.

280 The cited methods for wave reflection estimation have been applied here
 281 for the analysis of wave motion in front of the OWC device described in
 282 Section 2. The results for three- and four- probe methods are shown in Fig-
 283 ure 5 for all the tests carried out. Wave length L_p is estimated by means of
 284 dispersion relation for peak wave period T_p and still water depth h at the
 285 wavemaker. It can be noted that the results from three- and four- probe
 286 methods provides reflection coefficient values which range between 0.4 and
 287 0.9. Generally these two methods give most similar values of reflection co-
 288 efficient. The four- probe method gives most reliable values [38]. Thus only
 289 the four-probe method results are considered in the remaining part of this
 290 paper.

291 3.2. *Reflection coefficient*

292 The estimation of total reflection coefficient, for all the random wave
 293 tests, allows the study of the effect of the geometric parameters varied in
 294 the experiments, i.e. orifice diameter and still water depth. In the present
 295 analysis, two dimensionless parameters which affect the wave motion have
 296 been identified in order to maximize the applicability of the experimental
 297 results to other OWC configurations having similar shape.

298 As regards the orifice dimension, it is possible to note that the air flows
 299 in the OWC system are forced by changes in free surface elevation inside
 300 the chamber and constrained by the orifice restriction. Since the flow is
 301 regulated by the orifice area, the orifice diameter (d_0) has been replaced, in
 302 the following analysis, by the relative orifice surface area defined as the ratio

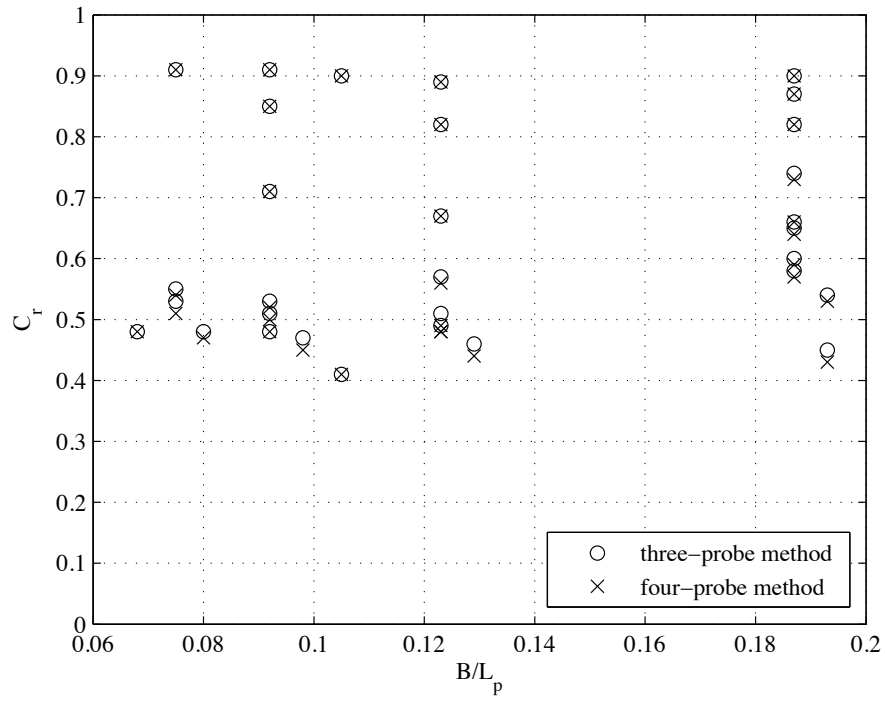


Figure 5: Evaluated reflection coefficients C_r , in front of OWC device, as function of relative chamber width B/L_p . The circle and cross symbols denote results of three- and four-probe methods respectively. Clusters of circles and crosses indicate that three- and four-probe methods are working similarly.

303 between orifice area and chamber's horizontal cross-sectional area:

$$A_0/A_c = \frac{\pi(d_0/2)^2}{BB_t} \quad (6)$$

304 Such a dimensionless parameter, obtained on the basis of the system ge-
 305 ometries defined in Table 1, ranges between 0 and 2% for the configurations
 306 tested at GWK, as it is summarized in Table 3.

307 Still water depth variation may affect wave-air dynamics at OWC by
 308 means of the draft (a) of the frontal “curtain” wall. Thus the draft can be
 309 related to the still water depth at the OWC entrance (d) by introducing a
 310 dimensionless parameter a/d which represents the relative draft of the frontal
 311 wall.

312 Both dimensionless parameters A_0/A_c and a/d , related to surface orifice
 313 and frontal wall draft respectively, have been used in Figure 6 for the analysis
 314 of total reflection coefficient as function of relative caisson width (B/L_p).
 315 As regards the orifice influence on wave motion, it is no surprise that the
 316 reflection coefficient is near to 0.9 when the air conduct is closed, i.e. $A_0/A_c =$
 317 0, in agreement with the formulation proposed in [41] for plain vertical wall
 318 demonstrating that the OWC chambers do not dissipate wave energy when
 319 air does not flow into or out of the device.

320 For non zero values of orifice area, the total reflection coefficient decreases.
 321 In particular, Figure 6(a) shows that the reduction of reflection coefficient
 322 is evident even for the smallest non zero value of relative surface orifice,
 323 i.e. $A_0/A_c = 0.1\%$. As expected, the behaviour of reflection coefficient is
 324 not monotonic with respect to orifice dimensions: it decreases until relative
 325 surface orifice is equal to 0.9%, after that an increase of wave reflection effect
 326 is noticeable, for $A_0/A_c = 2\%$.

Table 3: Dimensionless parameter for the tested conditions: relative orifice surface area A_0/A_c , with of caisson over peak wave length B/L_p , significant incident relative wave height $H_s^* = H_{m0,i}/h$, relative draft of frontal wall a/d .

Test number	A_0/A_c [%]	B/L_p	H_s^*	a/d
1; 2; 3; 4; 5	0; 0.1; 0.2; 0.9; 2.0	0.19	0.07	0.37
6	0.9	0.19	0.11	0.37
7; 8	0; 0.9	0.19	0.15	0.37
9; 10; 11; 12	0.1; 0.2; 0.9; 2.0	0.19	0.11	0.37
13; 14	0; 0.9	0.19	0.17	0.37
15	0.9	0.12	0.23	0.37
16; 17	0; 0.9	0.12	0.07	0.37
18; 19; 20; 21; 22	0; 0.1; 0.2; 0.9; 2.0	0.12	0.15	0.37
23	0.9	0.12	0.23	0.37
24; 25	0; 2.0	0.11	0.19	0.37
26	0.9	0.09	0.29	0.37
27	0.9	0.09	0.11	0.37
28	0.9	0.09	0.09	0.07
29	0.9	0.07	0.17	0.07
30	0.9	0.07	0.20	0.07
31	0.9	0.07	0.18	0.07
32	0.9	0.07	0.22	0.07

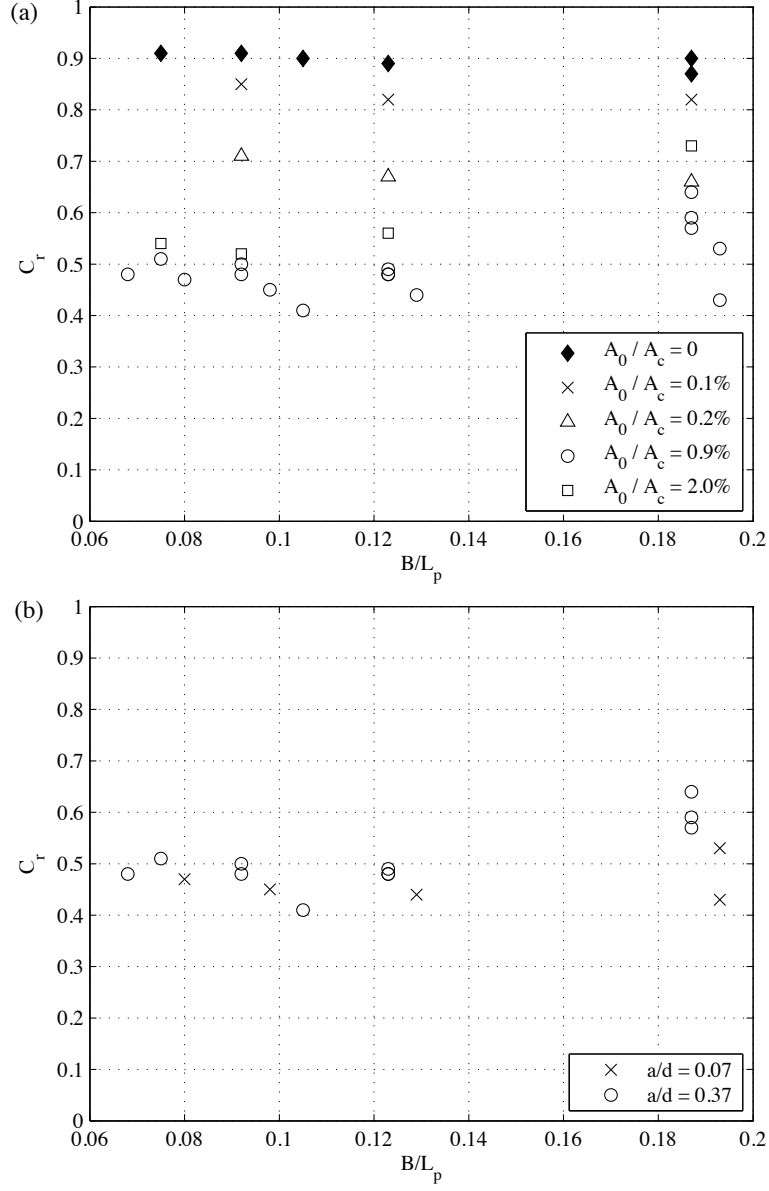


Figure 6: Reflection coefficients C_r as function of relative chamber width B/L_p : (a) influence of orifice relative area A_0/A_c ; (b) influence of relative draft of frontal wall a/d , for $A_0/A_c = 0.9\%$.

327 The efficiency of the OWC device (i.e. chamber air energy over incident
328 wave energy) and the reflection coefficient are strictly related to each other.
329 They have an opposite behavior, as it is possible to demonstrate on the
330 basis of energy balance arguments, see for example Tseng et al. [28]. As
331 a consequence, an optimized orifice opening is believed to give both the
332 maximum energy conversion efficiency and minimum wave reflection.

333 The effect of orifice variation on OWC efficiency has been investigated by
334 Thiruvankatasamy & Neelamani [42] and, more recently, by Ashlin et al. [43].
335 In both studies the optimum dimensionless orifice opening, which gives the
336 greatest efficiency, ranges between 0.6% and 0.9%. Such values are similar
337 to the optimum orifice obtained here, again minimizing wave reflection.

338 The physical meanings of these optimum values are related. In detail, the
339 damping at the orifice is higher for any opening smaller than the optimum,
340 causing greater absolute values of relative air pressure (in both compression
341 and decompression steps) and smaller water surface oscillations into the
342 chamber, so leading to a reduction of efficiency, as reported in Ashlin et al.
343 [43]. The increase of wave reflection for opening smaller than the optimum
344 is also due to the greater air pressure inside the chamber, which reaches its
345 maximum for closed orifice.

346 If an orifice opening is greater than its optimum, Thiruvankatasamy &
347 Neelamani [42] found that the absolute values of relative air pressure decrease
348 so causing reduction of efficiency, notwithstanding the increase of free surface
349 oscillation inside the chamber. Such an higher free surface oscillation causes
350 the increase of wave reflection seen in these GWK tests.

351 Since the wave reflection is inversely related to the efficiency of the sys-

tem in converting wave energy, the value 0.9% of relative surface orifice represents an optimum in this OWC device's characteristics. For this reason, the $A_0/A_c = 0.9\%$ configuration has been studied more fully, as can be seen in Figure 6(a) and in the Table 2.

The behaviour of reflection coefficient, as function of relative width of the caisson, shows an inverse relation for smallest values of non-zero orifice dimension, i.e. for $0 < A_0/A_c \leq 0.2\%$. When the orifice opening is equal or greater than its optimum value ($A_0/A_c = 0.9\%$), a proportional relationship can be seen between C_r and B/L_p for relative width greater than 0.11. Between these, a marginally reduced reflection coefficient is observed for values of relative width near to 0.11.

A focus on C_r behaviour for the optimum orifice is shown in Figure 6(b) by varying the draft of the front wall. Reflection coefficients are slightly lower for small drafts, particularly evident for $B/L_p > 0.11$, i.e. for the shortest waves. The physical explanation may be related to the fact that the shorter period waves have orbital velocities which decrease most rapidly toward the bottom. Thus the lower the front wall (and thus the smaller the opening), the less intense is the wave motion into the OWC caisson, and the greater the reflected wave height. When however the front wall is shallow, and the opening greatest, then the reflection coefficient may increase as the incident waves act more on the rear wall.

The influence of incident wave characteristics on wave motion reflected by the OWC device has been studied by means of the spectral reflection coefficient $C_{r(f)}$, defined for each wave frequency f . Figure 7(a) shows the effects of peak wave period variation, through the relative width of caisson

377 calculated using the peak wave length (B/L_p). For each frequency compo-
 378 nent, the spectral reflection coefficient, $C_{r(f)}$, is plotted against the relative
 379 chamber width B/L , for that frequency component's wavelength L at water
 380 depth h from the flume floor. In Figure 7(a) all data have a fixed significant
 381 incident relative wave height $H_s^* = H_{m0,i}/h = 0.11$, such that the influence
 382 of peak wave length upon $C_{r(f)}$ is isolated. This value for H^* has been se-
 383 lected since it represents a median value between those tested, for which wave
 384 breaking does not take place. It is possible to observe that all the spectral re-
 385 flection coefficients approach their minimum values, for $0.10 < B/L < 0.15$,
 386 relatively independently of the characteristics of incident waves. This agrees
 387 with results of physical modelling of breakwaters with perforated caisson
 388 having non-homogeneous porosity [e.g. 38, 44].

389 In the rest of the domain, the function $C_{r(f)}$ is more influenced by the
 390 relative width of caisson B/L_p . For each B/L_p a different maximum is found,
 391 with apparent values of reflection greater than 1. Such 'unphysical' behaviour
 392 may be an indication of energy transfer between wave frequencies. Since wave
 393 energy conversion in the OWC system is related to both water and air motion,
 394 air flowing through the orifice is influenced by compression and hydrodynam-
 395 ics. In particular, the air flowing through the orifice (PTO) represents an
 396 oscillating motion which is the result of compression and expansion of air
 397 inside the chamber. Its behaviour is similar to a spring oscillating with a fre-
 398 quency which depends upon its geometry and the actions applied to it, i.e.
 399 the wave motion. The variation in time of wave characteristics in random
 400 waves influences the frequency of air intake and outflow. Air compressibility
 401 acts like a filter on the wave frequencies which are converted into air flow

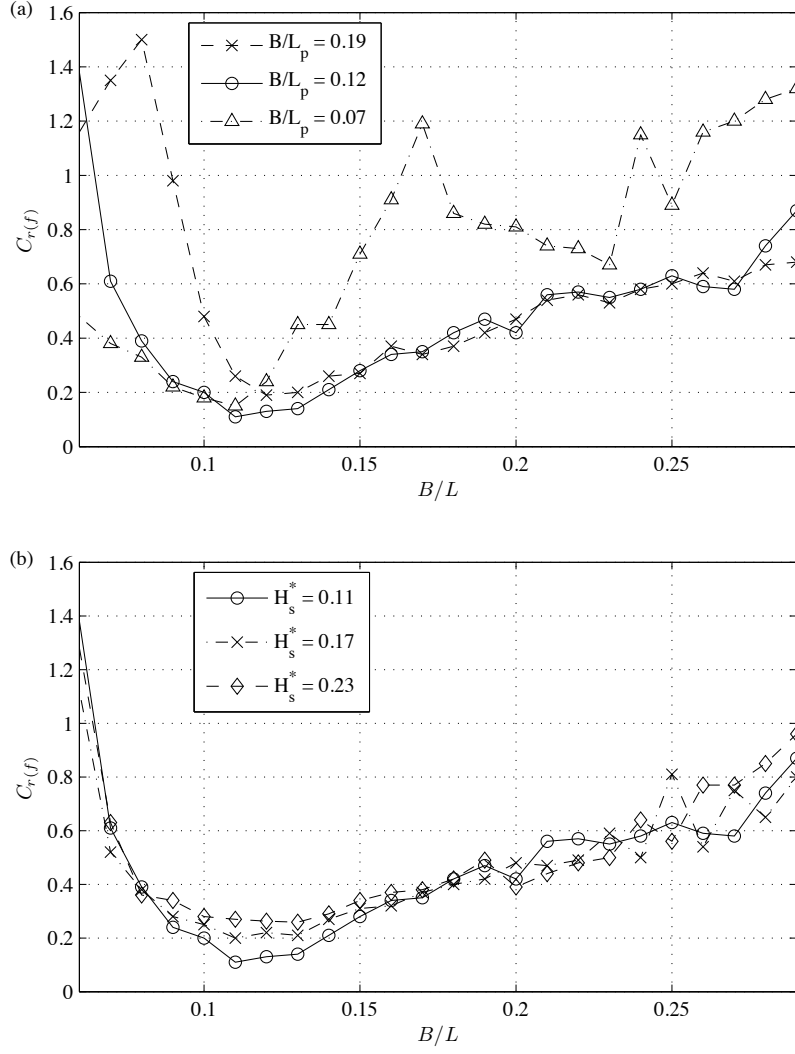


Figure 7: Spectral reflection coefficients $C_{r(f)}$ as function of B/L of each frequency component: (a) influence of peak wave period by means of peak relative width of caisson B/L_p for tests (n. 6, 11 and 27) with relative incident wave height $H_s^* = H_{m0,i}/h = 0.11$; (b) influence of relative incident wave height H_s^* for tests (n. 11, 14 and 15) with relative chamber width $B/L_p = 0.12$.

402 cycle frequencies. When the incident wave at OWC is not in phase with the
 403 air in/out flow, the air instantaneously adjusts its pressure and more slowly
 404 adjusts its frequency. The waves having near dominant (peak) frequencies
 405 are converted into air flow, thus they are partly absorbed by the system. On
 406 the contrary, several incident waves are unable to enter into the OWC since
 407 they are not in phase with the air motion. In the worst case, waves are in
 408 phase with pressure variation, thus retrieving pressure energy stored in the
 409 air chamber and not yet converted into air kinetic energy. For such frequen-
 410 cies, the amplitude of reflected wave component is greater than the incident
 411 one and the spectral coefficient $C_{r(f)}$ is greater than 1. As a consequence, the
 412 possibility of obtaining reflected waves greater than incident waves is strictly
 413 related to the possibility of storing energy inside the caisson by means of air
 414 pressure potential energy.

415 The behaviour of spectral reflection coefficient for fixed $B/L_p = 0.12$ and
 416 variable H_s^* is shown in Figure 7(b): the minimum values of $C_{r(f)}$ increase
 417 proportionally with H_s^* and they vary between 0.1 and 0.3. However the
 418 shapes of the $C_{r(f)}$ versus B/L distribution are quite similar to each other,
 419 indicating a relatively weak influence of wave height. Since non-linearity is
 420 often related to wave height, this last finding indicates that the air-water
 421 dynamics at the OWC can probably be linearized and can be related to wave
 422 period and chamber dimensions.

423 The low reflection coefficient obtained for the optimum orifice allows
 424 to consider the OWC integrated into breakwaters as a good alternative to
 425 Jarlan-type breakwaters. Further discussions on waves reflection at the OWC
 426 are reported in the last Section of the paper.

4. Loadings

4.1. Data analysis

Pressure transducers were installed in the OWC caisson to measure loadings on the front wall, on the rear wall and in the ceiling (see Figure 3). Each transducer is logged at a frequency of 1000 Hz in order to adequately describe impulsive loadings. Forces on the caisson have been computed by integrating pressure on the three surfaces with transducer arrays. In particular, the force at the front wall has been obtained by considering only the wet surface. The height of such a wet surface has been linearly extrapolated on the basis of the free surface elevations measured at the two wave gauges nearest to the front wall. At the top of that wall the (relative) pressure is assumed to be zero. At the bottom of the front wall, and at all the corners of the two internal walls (i.e. roof and rear wall), the pressures have been assumed to be equal to that registered by the nearest pressure sensor. In such a way the pressures are defined along each wall in which pressure sensors are located. The force at each wall is computed as the sum of the trapezoid areas delimited by the linear pressure distributions along that wall, multiplied by the transverse width of the OWC.

At negative pressures, and immediately around the moment of zero down crossing, the pressure signals exhibited an unphysical oscillation (see for example the time series shown in Figure 8). A filter has been developed and applied which acts only when loads down-cross the zero value for more than one time-step. Thus, the maximum actual peaks have not been modified by filtering procedure because they are always surrounded by positive values.

The pressure-time signals have been truncated with the removal of the

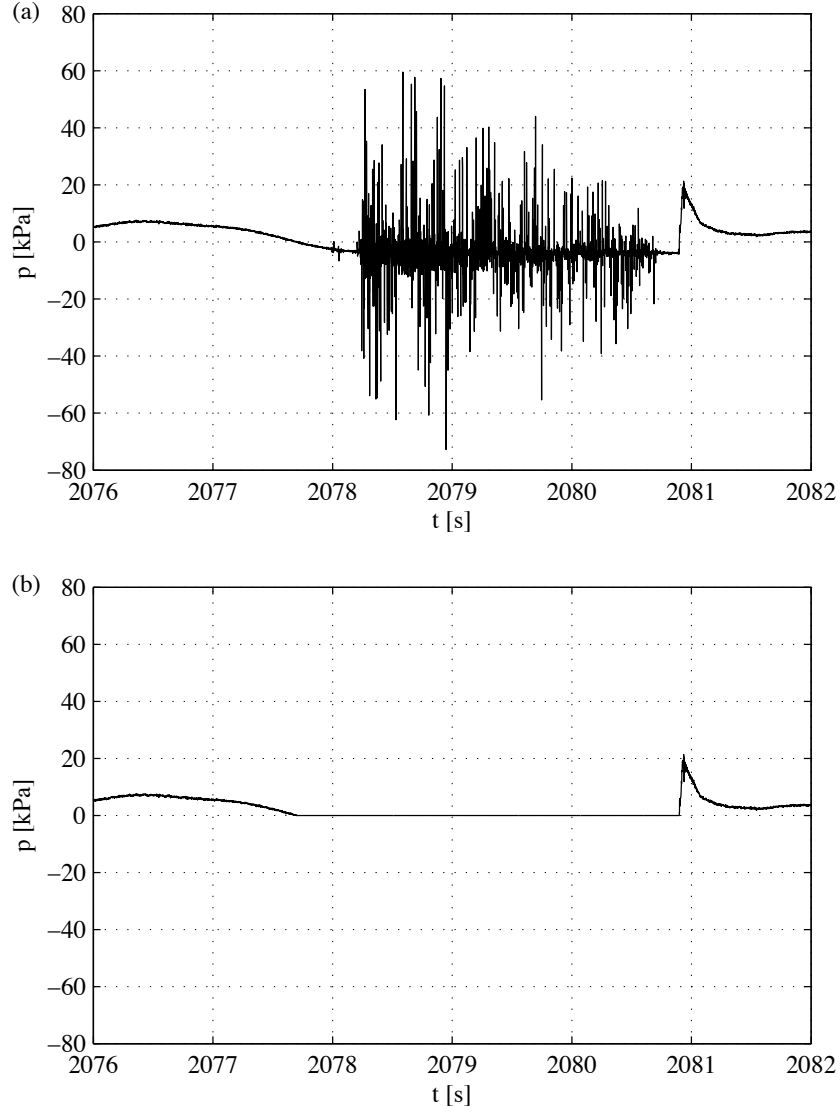


Figure 8: Pressure signal registered by transducer n.1, placed on frontal wall at height 3.09 m from the bottom of the channel. Test condition n.26: $T_p = 6.0$ s, $H_s = 1.0$ m, $d_0 = 0.2$ m; (a) unfiltered signal; (b) filtered signal.

early part until such time as the wave conditions are properly established. The time of the signal, taken into account for the following data analysis, corresponds to a nominal 1000 waves for each probe. Maximum loadings have been computed by establishing the four maximum values of the forces at the wall, the averages of which give the 1/250 forces. Values of the circumscribing 1/250 pressures have been computed by extracting for each transducer the 4 values corresponding to the 4 largest wave forces. This procedure yields maximal values for the 1/250 pressure distributions.

In this approach however, the maximum loadings on each wall are not extracted at the same instant; so the maximum values of force (and pressures) at each wall may be related to different waves or to different phases of the same wave.

4.2. Pressures

The results of the procedure to identify 1/250 pressures at the OWC caisson are here analyzed by considering the dimensionless pressure $p/(\rho g H_{m0,i})$ and the dimensionless axes x/B and z/d . Such analysis is focused on the widely tested optimum orifice $A_0/A_c = 0.9\%$.

The maximum (1/250) pressure distribution on the external front wall is reported in Figure 9. It is compared with the ‘extended Goda’ formulation [45] for impulsive loadings on plain vertical walls.

Both the influence of wave period and wave height are considered, by means of parameters B/L_p and $H_s^* = H_{m0,i}/h$, respectively. In all the tests, the measured pressure distributions are similar to that computed, with the peak value located near the still water level, i.e. at $z/d = 0$. The match with Goda predictions is quite good for small wave heights, $H_s^* = H_{m0,i}/h \leq 0.11$,

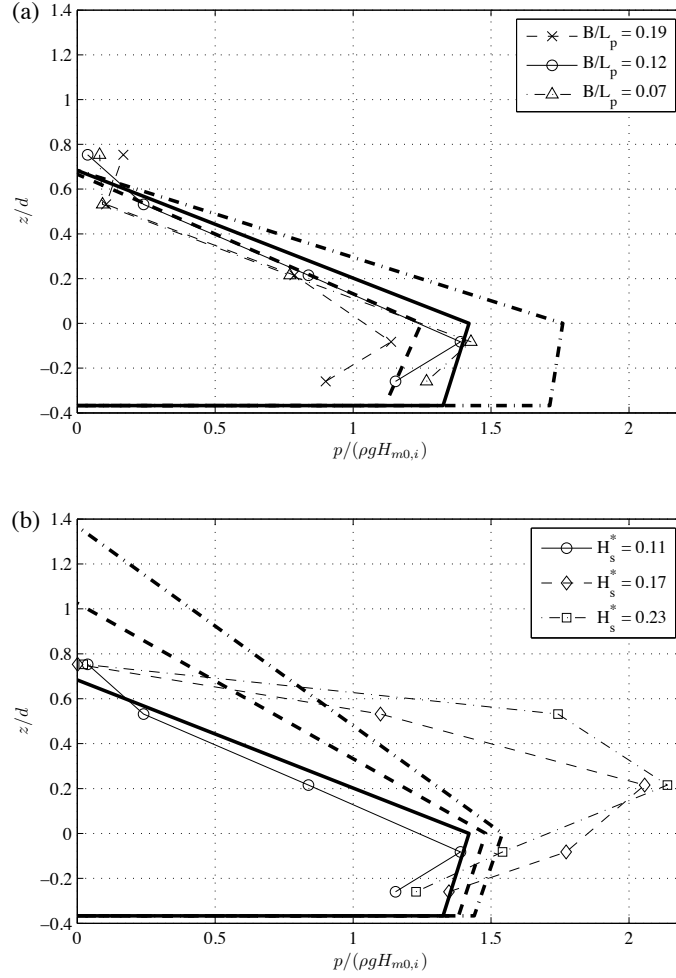


Figure 9: Recorded and estimated maximum dimensionless pressure ($1/250$) on the front wall; pressures recorded by transducers are reported in markers; results of ‘extended Goda’ formulation [45] are shown in thick lines (without markers), having the same hatch of the measured pressures: (a) influence of peak wave period by means of B/L_p (dash line: 0.19, continuous line: 0.12, dash-dot line: 0.07) for fixed $H_s^* = H_{m0,i}/h = 0.11$; (b) influence of relative incident wave height H_s^* (continuous line: 0.11, dash line: 0.17, dash-dot line: 0.23) for $B/L_p = 0.12$.

477 with a slight over-prediction of pressures by the ‘extended Goda’ formulation.
 478 As wave heights increase, the pressure peak is shifted upwards, as is shown
 479 in Figure 9(b).

480 Such behaviour is not captured by the ‘extended Goda’ formulation,
 481 which therefore under-estimates pressures for $z/d > 0$. On the contrary,
 482 the pressures under the still water level give slightly lower values than pre-
 483 dicted. The ‘extended Goda’ formulation cannot be compared with measured
 484 pressure data for $z/d \leq -0.4$ because in this point the pressure drops to zero
 485 due to the presence of the frontal wall opening.

486 Measured pressure distributions (1/250) inside the caisson, on the rear
 487 wall are illustrated in Figure 10 for varying peak wave length and incident
 488 wave height. Such distributions have been compared with a formulation
 489 developed by Takahashi & Shimosako [46] for loadings within a perforated
 490 wall caisson. Notwithstanding some evident geometrical differences between
 491 OWC and perforated caissons, predicted distributions are qualitatively sim-
 492 ilar to those measured inside the OWC caisson: the pressures increase from
 493 the bottom and reach a maximum near the still water level, after which they
 494 reduce towards the roof. For lower wave heights, pressures measured on the
 495 rear wall of the OWC chamber are generally smaller than might be predicted.
 496 Conversely, for more impulsive wave conditions, $H_s^* \geq 0.17$, pressures at or
 497 above the static water level exceed predictions. The pressures are similar to
 498 those measured on the front wall for the same wave conditions.

499 Finally the pressure distribution on the chamber ceiling, reported in Fig-
 500 ure 11, show a uniform shape for non-impulsive wave conditions ($H_s^* = 0.11$).
 501 The pressures measured in these cases are therefore of the air, compressed in

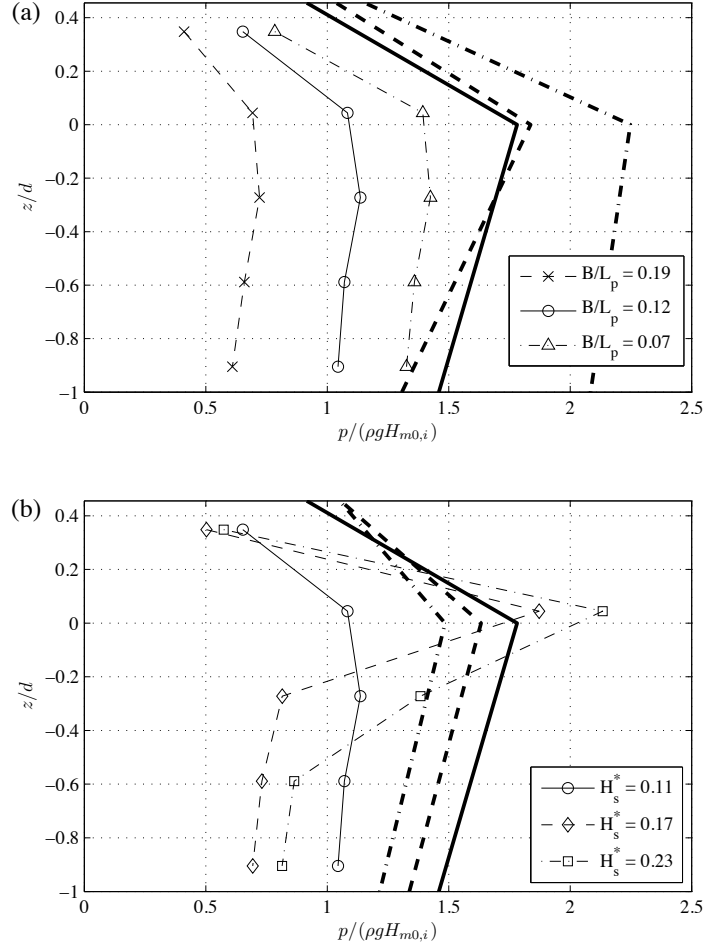


Figure 10: Maximum dimensionless pressure ($1/250$) distributions on the rear vertical wall; results of perforated wall caisson Takahashi & Shimosako formulation [46] are shown in thick lines; (a) influence of peak wave period by means of B/L_p (dash line: 0.19, continuous line: 0.12, dash-dot line: 0.07) for fixed $H_s^* = H_{m0,i}/h = 0.11$; (b) influence of relative incident wave height H_s^* (continuous line: 0.11, dash line: 0.17, dash-dot line: 0.23) for $B/L_p = 0.12$.

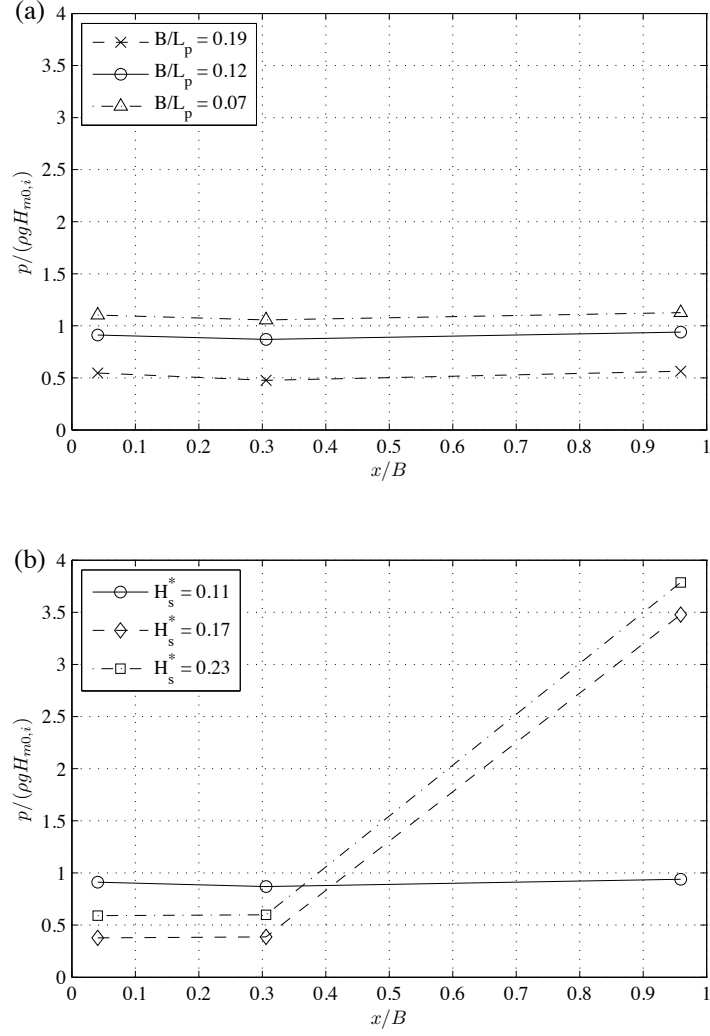


Figure 11: Maximum dimensionless pressure ($1/250$) distribution at the roof of the caisson, obtained from pressure sensors P6, P13 and P7, placed at $x/B = 0.04$, 0.31 and 0.96 respectively; (a) influence of peak wave period by means of peak relative width of caisson B/L_p for fixed $H_s^* = H_{m0,i}/h = 0.11$; (b) influence of relative incident wave height H_s^* for $B/L_p = 0.12$.

the upper part of the chamber. Figure 11(a) shows that these pressures are little influenced by wave period, and are inversely related to B/L_p .

If the incident wave height increases, a peak of pressure is encountered at the rear corner of the roof, as it is shown in Figure 11(b). This is probably caused by a jet on the rear wall hitting the chamber roof. It is important to highlight that the width of the jet is not caught by the available experimental data. Pressures measured on the rest of the roof are lower than those obtained for non-impulsive waves. It is likely therefore that this jet is related to instabilities in the OWC chamber that do not significantly pressurise air in the chamber, so may adversely affect the efficiency as a WEC.

The presence of jet inside the chamber has been observed during the tests and it would probably cause problems to any air turbine.

4.3. Forces

Measured maximum forces, defined as 1/250 of the peak forces acting on the OWC caisson, are analyzed here for all the random wave conditions tested. The effects of incident wave height and of orifice opening have been investigated by means of the dimensionless parameters H_s^* and A_0/A_c , respectively.

Measured forces on the frontal wall have been compared with forces predicted by the ‘extended Goda’ method for vertical walls [45], as for the pressure distribution discussed previously. Figure 12 shows the ratio between measured and predicted forces as function of relative wave height, for all the orifice openings tested. The horizontal solid line represents exact agreement between measured and predicted forces: the points below such a line correspond to over-predicted cases; the points above the line are unsafe, since

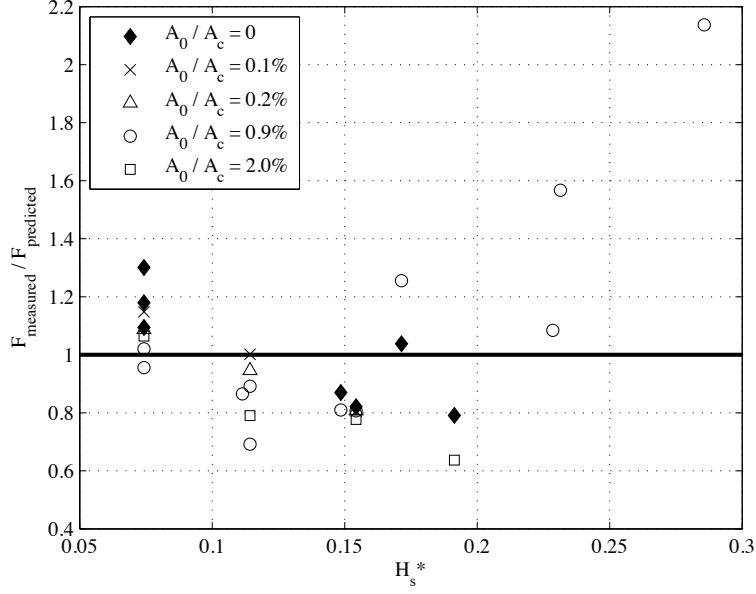


Figure 12: Ratio between measured and predicted forces (1/250) at the external frontal wall, by applying the ‘extended Goda’ formulation [45]. Influence of relative incident wave height ($H_s^* = H_{m0,i}/h$) and of orifice surface ratio A_0/A_c . Solid line represents the best mean fit.

the adopted formulation gives lower values of force with respect to those measured.

The results suggest that the maximum forces are inversely related to orifice opening. The relative error is below 40% when $H_s^* < 0.2$, independent of orifice opening. In particular, Goda formulation overestimates the measured force for $H^* = 0.11$ ($F_{\text{measured}}/F_{\text{predicted}} < 1$), i.e. for low impulsive waves. Such a behaviour is in accordance to what shown in Figure 9(b), where the pressures measured are always lower than Goda prediction for $H^* = 0.11$. When H^* increases the pressure overcomes the Goda predictions since impul-

536 sive effects are more intense. For $0 < H^* < 0.11$ Figure 12 show a decrease
 537 of the ratio $F_{measured}/F_{predicted}$ as function of H^* which does not correspond
 538 to a decrease of force (and/or pressure): it is only an underestimation of the
 539 Goda formula, which is probably related to the reduction of scale effects in
 540 large wave flume (GWK), compared to Goda experiments. However the pres-
 541 sures and forces at the front wall always increase with H^* , as it is physically
 542 expected.

543 When the relative wave height increases, $H_s^* > 0.2$, forces increase and
 544 the simplified predictions become unsafe.

545 As regards the internal rear vertical wall, the ratio between measured and
 546 predicted force is shown in Figure 13, using the perforated caisson prediction
 547 method by Takahashi & Shimosako [46]. The forces are generally inversely
 548 related to orifice opening, with the exception of a case for which relative
 549 incident wave height is near to 0.18. It is noted that the method adopted
 550 was not developed for OWC caissons. Even so, the method generally gives
 551 greater predicted forces than those measured, particularly for optimum orifice
 552 ($A_0/A_c = 0.9\%$). On the contrary, loads on the rear wall are greater for orifice
 553 openings smaller or larger than the optimum.

554 Dimensionless forces on the ceiling of the chamber at 1/250 level are
 555 shown in Figure 14, suggesting general increases with increasing relative wave
 556 height H_s^* . An optimum orifice opening appears to lead to significantly lower
 557 internal loadings relative to those measured for smaller or larger orifices.

558 It is worth highlighting that the maximum dimensionless force is mea-
 559 sured under conditions with the largest orifice, rather than under closed
 560 orifice conditions. The likely explanation is that under the closed orifice con-

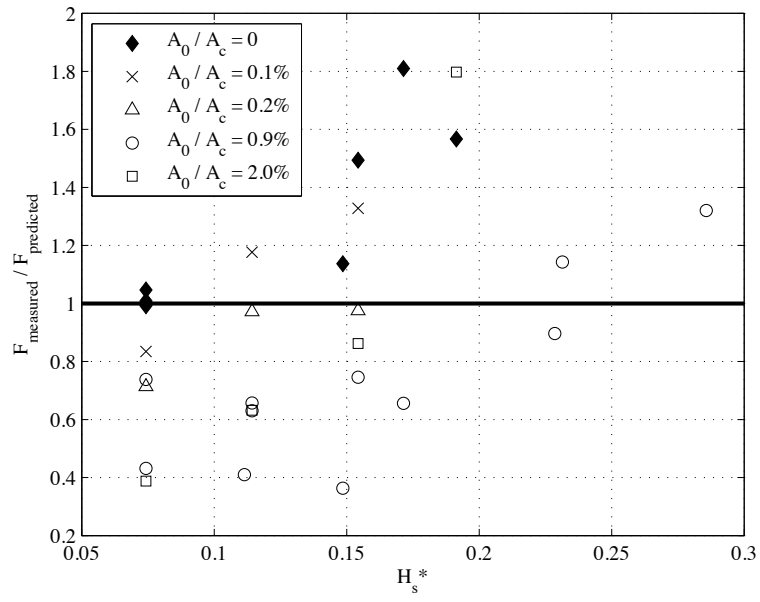


Figure 13: Ratio between measured and predicted forces (1/250) at the internal rear wall, by applying the perforated wall caisson formulation [46]. Influence of relative incident wave height ($H_s^* = H_{m0,i}/h$) and of orifice surface ratio A_0/A_c . Tick line represents the best fit, the points over such a line are unsafe with the adopted formulation.

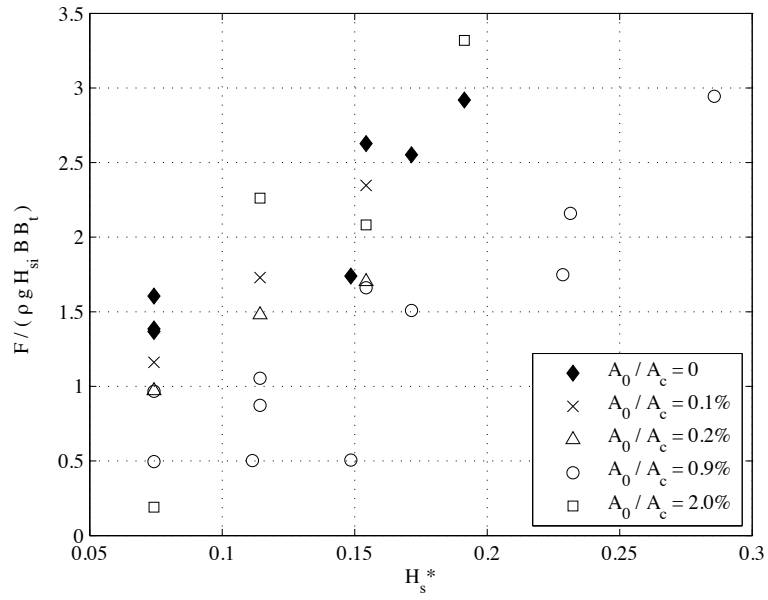


Figure 14: Measured dimensionless maximum forces ($1/250$) at the roof. Influence of relative incident wave height ($H_s^* = H_{m0,i}/h$) and of orifice surface ratio A_0/A_c .

561 ditions, there is little movement of the water inside the chamber, mitigating
562 strongly against the formation of the type of jet responsible for the much
563 larger rear-wall and chamber ceiling pressures and forces. It is clear however
564 that conditions that lead to pulsating motions within the OWC chamber
565 therefore pressurise the air in the chamber relatively uniformly. Conversely,
566 conditions that cause sloshing within the chamber are more likely to give rise
567 to impacts on the rear wall and on the ceiling of the chamber.

568 5. Conclusions

569 The aim of this work is to provide useful information contributing to the
570 design of OWC systems integrated into vertical breakwaters, with particu-
571 lar attention to wave reflections and loadings on the front wall, rear wall,
572 and on the ceiling of the chamber. The results obtained allow the consid-
573 eration of the OWC breakwater as a possible alternative to composite and
574 perforated caissons to reduce reflections which affect the classic vertical wall
575 breakwaters. In such a context the energy production is a complementary as-
576 pect and will be addressed in future publication, by considering the complex
577 interaction between air flow and a power take off (PTO).

578 Large scale experiments in the GWK, carried out under random wave
579 conditions, have explored the effects of: orifice restriction (i.e. PTO); water
580 depth, and wave conditions on wave motion, by means of suitably defined
581 dimensionless variables.

582 In detail, relative orifice area affects significantly the total reflection coef-
583 ficient which reaches a maximum, equals $C_r \approx 0.9$, when the orifice is closed.
584 This agrees with the literature for reflection of random waves from vertical

walls. Moreover the minimum of reflection is not reached for the largest tested orifice but for an optimum condition. For tests reported here, this optimum was found when the relative orifice surface is equal to 0.9%, from which reflection coefficient $C_r \approx 0.5$. Such an orifice maximises the capacity of the system to convert wave energy into air kinetic energy.

The variation of still water depth, for fixed OWC geometry, affects wave motion by means of draft variation of the frontal wall: reflection coefficient is found to increase with wall draft and, consequently, with still water depth.

The influence of incident significant wave height and peak wave period on both spectral reflection coefficient and pressure distribution have been investigated. It has been found that all the spectral reflection coefficients reach a minimum when the relative width of the caisson chamber $B/L \approx 0.10 - 0.15$. This agrees with physical models results for non-homogeneous perforated wall breakwater.

The OWC system presents similar aspects to Jarlan-type breakwaters. Such analogy has been verified also in the loading estimation, indeed a formulation has been considered for prediction of pressure distribution inside the caisson which was developed for perforated breakwater. It has been shown that the predicted shape of pressure distribution is qualitatively similar to that measured along the rear vertical wall, i.e. the maximum pressure is located near the still water level.

The loading measured on the frontal external wall, compared with the ‘extended Goda’ formulation for vertical wall, shows differences less than 40% when the relative wave height $H_s^* \leq 0.2$. After that the error increases and the considered formulation becomes unsafe.

610 Measurements of pressure on the ceiling of the caisson give uniform values
611 for low significant wave heights and a spike at the rear corner for the highest
612 incident waves. This last behaviour is related to the presence of a jet within
613 the chamber, caused by a breaking wave which impacts the real wall, as
614 observed by the internal camera during testing. Such jets may cause problems
615 to air turbine that may be installed at the OWC. Thus, a system have to be
616 introduced for deflecting these upwards jets away from the air duct to the
617 turbine. The OWC turbine should to be closed when near breaking wave
618 conditions appear, both for the safety of the chamber structure and of the
619 turbine

620 **Acknowledgments**

621 The authors are grateful to HR Wallingford, the University of Edinburgh,
622 Second University of Naples, Queen's University of Belfast, University of East
623 Anglia for supporting the staff time devoted to this project. Access to the
624 GWK has been supported by European Community's Seventh Framework
625 Programme through the grant to the budget of the Integrating Activity
626 HYDRALAB IV within the Transnational Access Activities, Contract no.
627 261520. The authors would also like to thank Dr Matthias Kudella and Dr
628 Stefan Schimmels and their support team at the GWK for their cheerfulness,
629 tolerance and considerable assistance in the design evolution, model
630 construction, and testing. Important input from Professor Trevor Whittaker
631 (Queen's Belfast) and Dr Mark Cooker (Univ. East Anglia) in the study
632 design is gratefully acknowledged. Assistance in the testing and supporting
633 physical and numerical modelling from Nic Miller and David Bourke (Uni-

634 versity of Edinburgh), Mariangela Sfouni-Grigoriadou, Encarnacion Median-
 635 Lopez, Giovanni Cuomo, Aggelos Dimakopoulos and Daniele Longo (HR
 636 Wallingford), Vincenzo Ferrante (Second University of Naples) is also grate-
 637 fully acknowledged.

638 References

- 639 [1] R. A. Arinaga, K. F. Cheung, Atlas of global wave energy from 10 years
 640 of reanalysis and hindcast data, *Renewable Energy* 39 (1) (2012) 49–64.
 641 doi:10.1016/j.renene.2011.06.039.
- 642 [2] K. Gunn, C. Stock-Williams, Quantifying the global wave
 643 power resource, *Renewable Energy* 44 (2012) 296–304.
 644 doi:10.1016/j.renene.2012.01.101.
- 645 [3] F. Arena, V. Laface, G. Malara, A. Romolo, A. Viviano, V. Fiamma,
 646 G. Sannino, A. Carillo, Wave climate analysis for the design of wave en-
 647 ergy harvesters in the Mediterranean Sea, *Renewable Energy* 77 (2015)
 648 125–141. doi:10.1016/j.renene.2014.12.002.
- 649 [4] D. Vicinanza, P. Contestabile, V. Ferrante, Wave energy potential in
 650 the north-west of Sardinia (Italy), *Renewable Energy* 50 (2013) 506–
 651 521. doi:10.1016/j.renene.2012.07.015.
- 652 [5] C. Iuppa, L. Cavallaro, D. Vicinanza, E. Foti, Investigation of suitable
 653 sites for wave energy converters around Sicily (Italy), *Ocean Science*
 654 11 (4) (2015) 543–557. doi:10.5194/os-11-543-2015.

- 655 [6] M. Monteforte, C. L. Re, G. Ferreri, Wave energy assess-
656 ment in Sicily (Italy), *Renewable Energy* 78 (2015) 276–287.
657 doi:10.1016/j.renene.2015.01.006.
- 658 [7] A. F. Falcao, Wave energy utilization: A review of the technologies,
659 *Renewable and Sustainable Energy Reviews* 14 (3) (2010) 899–918.
660 doi:10.1016/j.rser.2009.11.003.
- 661 [8] K. Koca, A. Kortenhuis, H. Oumeraci, B. Zanuttigh, E. Angelelli,
662 M. Cantù, R. Suffredini, G. Franceschi, Analysis of wave reflection from
663 wave energy converters installed as breakwaters in harbour, in: *Proceed-*
664 *ings of the 10th European Wave and Tidal Energy Conference*, 2013.
- 665 [9] B. Zanuttigh, E. Angelelli, G. Bellotti, A. Romano, Y. Krontira,
666 D. Troianos, R. Suffredini, G. Franceschi, M. Cantù, L. Airoidi, F. Zago-
667 nari, A. Taramelli, F. Filipponi, C. Jimenez, M. Evriviadou, S. Broszeit,
668 Boosting blue growth in a mild sea: Analysis of the synergies produced
669 by a multi-purpose offshore installation in the northern adriatic, italy,
670 *Sustainability* 7 (6) (2015) 6804–6853. doi:10.3390/su7066804.
- 671 [10] S. Takahashi, Hydrodynamic characteristics of wave-power-extracting
672 caisson breakwater, in: *Twenty-First Coastal Engineering Conference;*
673 *Costa del Sol, Malaga, Spain, 1988*, pp. 2489–2503.
- 674 [11] S. Takahashi, H. Nakada, H. Ohneda, M. Shikamori, Wave power con-
675 version by a prototype wave power extracting caisson in sakata port, in:
676 *Proc. of 23rd International Conference on Coastal Engineering*, ASCE,
677 New York, 1992, pp. 3440–3453.

- 678 [12] V. Raju, S. Neelamani, Concrete caisson for a 150 kW wave energy pilot
679 plant: design, construction, and installation aspects, in: Proc of 2nd Int.
680 Offshore and Polar Eng. Conf., 1992, pp. 584–591.
- 681 [13] C. B. Boake, T. J. T. Whittaker, M. Folley, H. Ellen, Overview and
682 initial operational experience of the LIMPET wave energy plant, in:
683 12th International Offshore and Polar Engineering Conference, Kyushu,
684 Japan, Vol. 1, 2002, pp. 586–594.
- 685 [14] P. Boccotti, On a new wave energy absorber, Ocean Engineering 30
686 (2003) 1191–1200.
- 687 [15] C. Patterson, R. Dunsire, S. Hillier, Development of wave energy break-
688 water at Siadar, Isle of Lewis, in: Proc. Coasts, Marine Structures &
689 Breakwaters, Thomas Telford, London, 2009, pp. 738–749.
- 690 [16] Y. Torre-Enciso, I. Ortubia, L. L. de Aguilera, J. Marqus, Mutriku wave
691 power plant: from the thinking out to the reality, in: Proc 8th European
692 Wave and Tidal Energy Conf., Uppsala, Sweden, 2009, pp. 319–329.
- 693 [17] Y. Torre-Enciso, J. Marqus, L. L. de Aguilera, Mutriku. Lessons Learnt,
694 in: 3rd Int. Conf. on Ocean Energy, Bilbao, 2010.
- 695 [18] F. Neumann, I. L. Crom, Pico OWC - the Frog Prince of Wave En-
696 ergy? Recent autonomous operational experience and plans for an open
697 real-sea test center in semi-controlled environment, in: Proceedings of
698 the 9th European Wave and Tidal Energy Conference (EWTEC 2011),
699 Southampton, UK, 2011.

- 700 [19] F. Arena, A. Romolo, G. Malara, A. Ascanelli, On design and building
701 of a U-OWC wave energy converter in the Mediterranean Sea: a case
702 study, in: Proceedings of the 32nd International Conference on Ocean,
703 Offshore and Arctic Engineering OMAE2013, Nantes, France, 2013.
- 704 [20] M. Buccino, D. Banfi, D. Vicinanza, M. Calabrese, G. D. Giudice,
705 A. Carravetta, Non breaking wave forces at the front face of seawave slot-
706 cone generators, *Energies* 5 (2012) 4779–4803. doi:10.3390/en5114779.
- 707 [21] D. Vicinanza, J. H. Nørgaard, P. Contestabile, T. L. Andersen, Wave
708 loadings acting on overtopping breakwater for energy conversion, *Jour-
709 nal of Coastal Research Special Issue* 65 (2013) 1669–1674.
- 710 [22] D. Vicinanza, P. Contestabile, J. H. Nørgaard, T. L. Andersen, Innova-
711 tive rubble mound breakwaters for overtopping wave energy conversion,
712 *Coastal Eng.* 88 (2014) 154–170.
- 713 [23] M. Buccino, D. Vicinanza, D. Salerno, D. Banfi, M. Calabrese, Nature
714 and magnitude of wave loadings at seawave slot-cone generators, *Ocean
715 Engineering* 95 (2015) 34–58. doi:10.1016/j.oceaneng.2014.11.038.
- 716 [24] M. Buccino, D. Stagonas, D. V. anf G Muller, Development of a compos-
717 ite sea wall wave energy converter system, *Renewable Energy* 81 (2015)
718 509–522. doi:10.1016/j.renene.2015.03.010.
- 719 [25] E. Medina-Lopez, W. Allsop, A. Dimakopoulos, T. Bruce, Conjectures
720 on the failure of the owc breakwater at mutriku, in: *Coastal Structures*,
721 2015, p. 12.

- 722 [26] A. F. Falcao, J. C. Henriques, Oscillating-water-column wave energy
723 converters and air turbines: A review, *Renewable Energy* 85 (2016)
724 1391–1424. doi:j.renene.2015.07.086.
- 725 [27] G. Muller, T. J. Whittaker, Visualisation of flow conditions inside a
726 shoreline wave power-station, *Ocean Engineering* 22 (6) (1995) 629–641.
727 doi:10.1016/0029-8018(94)00032-3.
- 728 [28] R.-S. Tseng, R.-H. Wu, C.-C. Huang, Model study of a shore-
729 line wave-power system, *Ocean Engineering* 27 (8) (2000) 801–821.
730 doi:10.1016/S0029-8018(99)00028-1.
- 731 [29] B. Zanuttigh, L. Margheritini, L. Gambles, L. Martinelli, Analysis of
732 wave reflection from wave energy converters installed as breakwaters in
733 harbour, in: *Proceedings of the 8th European Wave and Tidal Energy*
734 *Conference*, 2009, pp. 384–392.
- 735 [30] R. Curran, T. P. Stewart, T. J. T. Whittaker, Design synthesis
736 of oscillating water column wave energy converters: Performance
737 matching, *Proceedings of the Institution of Mechanical Engineers*,
738 *Part A: Journal of Power and Energy* 211 (6) (1997) 489–505.
739 doi:10.1243/0957650981537375.
- 740 [31] I. Lopez, B. Pereiras, F. Castro, G. Iglesias, Optimisation of
741 turbine-induced damping for an OWC wave energy converter using
742 a RANS-VOF numerical model, *Applied Energy* 127 (2014) 105–114.
743 doi:10.1016/j.apenergy.2014.04.020.

- [32] Y.-S. Kuo, C.-S. Lin, C.-Y. Chung, Y.-K. Wang, Wave loading distribution of oscillating water column caisson breakwaters under non-breaking wave forces, *Journal of Marine Science and Technology* 23 (1) (2015) 78–87. doi:10.6119/JMST-014-0114-1.
- [33] M. Sainflou, Essai sur les digues maritimes verticales. (test on vertical sea dikes), *Annales des Ponts et Chaussees* 98 (1928) 5–48.
- [34] Y. Goda, A new method of wave pressure calculation for the design of composite breakwaters, *Proceeding of the Port and Harbour Research Institute, Ministry of Transport, Nagase, Yokosuka, Japan* (1973) 41–69.
- [35] S. J. Ashlin, S. A. Sannasiraj, V. Sundar, Wave forces on an oscillating water column device, *Procedia Engineering* 116 (2015) 1019–1026, 8th International Conference on Asian and Pacific Coasts (APAC 2015). doi:10.1016/j.proeng.2015.08.336.
- [36] W. Allsop, T. Bruce, J. Alderson, V. Ferrante, V. Russo, D. Vicinanza, M. Kudella, Large scale tests on a generalised oscillating water column wave energy converter, in: *Proceedings of the HYDRALAB IV Joint User Meeting, Lisbon, 2014*.
- [37] J. W. Weber, Representation of non-linear aero-thermodinamic effects during small scale physical model of OWC WECs, in: *Proceeding of the 7th European Wave and Tidal Energy Conference, 2007*.
- [38] C. Faraci, P. Scandura, E. Foti, Reflection of sea waves by combined caissons, *Journal of Waterway, Port, Coastal, and Ocean Engineering* 141 (2) (2015) 04014036. doi:10.1061/(ASCE)WW.1943-5460.0000275.

- 767 [39] E. Mansard, E. Funke, The measurement of incident and reflected spec-
768 tra using a least squares method, in: Proc. 17th Int. Coastal Engineering
769 Conf., ASCE, New York, 1980, pp. 154–172.
- 770 [40] Y. Goda, Y. Suzuki, Estimation of incident and reflected waves in ran-
771 dom wave experiments, in: Proc. 15th Int. Conf. Coastal Engineering,
772 ASCE, New York, 1976, pp. 828–845.
- 773 [41] W. Allsop, W. McBride, D. Colombo, The reflection performance of
774 vertical walls and low reflection alternatives: Results of wave flume tests,
775 in: Proceedings of the 3rd MCS Project Workshop, MAS2-CT92-0047,
776 Monolithic (Vertical) Coastal Structures, De Voorst, The Netherlands,
777 1994.
- 778 [42] K. Thiruvengatasamy, S. Neelamani, On the efficiency of wave en-
779 ergy caissons in array, Applied Ocean Research 19 (1997) 61–72.
780 doi:10.1016/S0141-1187(97)00008-4.
- 781 [43] S. J. Ashlin, V. Sundar, S. Sannasiraj, Effects of bottom pro-
782 file of an oscillating water column device on its hydrodynamic
783 characteristics, Renewable Energy 96, Part A (2016) 341 – 353.
784 doi:10.1016/j.renene.2016.04.091.
- 785 [44] K. J. McConnell, N. W. H. Allsop, D. M. Ethelston, Wave reflection from
786 coastal structures: development and application of new approaches, in:
787 Proceeding of the 10th Congress of Asia and Pacific Division of IAHR,
788 1996.

- 789 [45] S. Takahashi, K. Tanimoto, K. Shimosako, A proposal of impulsive
790 pressure coefficient for design of composite breakwaters, in: Proc. of
791 International Conference on Hydro-technical Eng. for Port and Harbor
792 Construction, Port and Harbour Res. Inst., 1994.
- 793 [46] S. Takahashi, K. Shimosako, Wave pressure on a perforated wall, in:
794 Proc. of International Conference on Hydro-technical Eng. for Port and
795 Harbor Construction, Port and Harbour Res. Inst., 1994.